

https://doi.org/10.1070/QEL17236

Optical fields in porous polylactide matrices

A.P. Sviridov, V.S. Zhigarkov, A.G. Shubnyi, V.I. Yusupov

Abstract. **Optical fields induced by laser light inside porous polymer matrices (scaffolds) under stimulating effect on cells are investigated. The spectra of light scattering coefficients and anisotropy factors of porous polylactide scaffolds in the visible and near-IR ranges are determined by numerical simulation based on experimental data obtained using a double integrating sphere. Studies are conducted for dry and wet scaffolds fabricated by supercritical fluid foaming and surface-selective laser sintering. The Monte Carlo method is used to calculate the fluence rate distribution under the assumptions of the Henyey–Greenstein phase scattering function and the model phase function of scattering on spherical cavities. It is shown that the fluence rate distribution mainly depends on the scattering coefficient and the mean cosine of the deflection angle (*g*-factor). The results obtained are of great practical importance for tissue engineering based on the use of polymeric porous scaffolds with cells to replace tissue defects; they can be used to determine the dose range for laser stimulation of cells.**

Keywords: *porous polymer matrix, scaffold, laser stimulation of cells, optical fields, numerical simulation.*

1. Introduction

One of the rapidly developing areas of modern medicine is tissue engineering [1, 2] based on the use of scaffolds with appropriate cells to replace defects in damaged tissues or entire organs. Initially, a tissue-engineered structure is formed [3], which is a scaffold. It ensures the necessary biomechanical properties of the corresponding tissue, provides structural support for cells, and creates the conditions for their metabolism and differentiation [4].

Cell metabolism in scaffolds is largely determined by a number of chemical and physical factors: the chemical structure of the material, local topography, architecture, and mechanical properties. Cellular life within a tissue-engineered construct is affected by diffusion restrictions on the delivery of oxygen and nutrients into the scaffold from the surrounding cultural environment. Thus, at depths from the surface exceeding the characteristic distance for oxygen diffusion (~100 μm [5]), there is a decrease in cell viability, a drop in cell population density and even cell death, as a rule, by the type of necrosis [6].

To overcome diffusion limitations, fluid is usually pumped through the scaffold (perfusion). Another effective method for improving the viability of cells in the volume of the cell construct is the photobiomodulation method, which consists in short-term exposure of biological objects to low-intensity monochromatic (laser) or non-monochromatic (LED-based) light in the visible and near-IR spectral regions [7–10]. It has been established that the result of photobiomodulation depends on the type of cells, as well as on the dose, intensity, temporal and spectral characteristics of the exposure [11]. It has been shown that a low-intensity exposure in the therapeutic dose range has a protective effect against various negative (oxygen [12] and nutritive [13] starvation) and damaging factors (from ultraviolet to ionising radiation) [14, 15]. Low-intensity (not leading to a temperature rise affecting the cells metabolism) optical light can cause a change in the proliferation rate of cells and affect their differentiation. Thus, it has been found in [16] that, when low-intensity laser light dose of 62.5 J cm^{-2} at λ = 635 nm is applied to stem neuronal cells placed in a gelatine–methacrylate matrix, cell proliferation increases significantly (by 44%) and differentiation increases at late stages of cultivation. We believe that the negative effect on the cells located in the scaffold depth, associated with the diffusion restriction on the delivery of oxygen and nutrients from the surrounding culture environment, can be largely levelled by photobiomodulation.

In the process of photobiomodulation, samples are usually irradiated by low-intensity light from one side. Due to the absorption and scattering of light in the matrix volume, the levels of irradiation of cells located in a three-dimensional scaffold can vary significantly. In this case, some cells are in many cases exposed outside the 'therapeutic range' of photobiostimulation. For near-surface cells, the intensity of incident light may prove to be higher than optimal, while for cells that are located far from the surface, on the contrary, lower. To evaluate this effect, it is necessary to know the fluence rate distribution in the entire scaffold volume. By difinition, the fluence rate is the energy of light quanta incident on the surface of a spherical volume element per unit time. That problem is solved by numerical calculation using experimentally obtained information on the effective optical properties of the scaffold material [17–20]. Similar calculations have been repeatedly conducted earlier for various strongly scattering media. In this work, we have simulated the fluence rate distribution in scaffolds designated for tissue engineering. As two model matrices, scaffolds formed on

A.P. Sviridov, V.S. Zhigarkov, A.G. Shubnyi, V.I. Yusupov
Institute of Photon Technologies, Federal Scientific Research Centre 'Crystallography and Photonics', Russian Academy of Science, ul. Pionerskaya 2, 108840 Moscow, Troitsk, Russia;
e-mail: sviridoa@gmail.com

Received 13 December 2019
Kvantovaya Elektronika **50** (1) 81–86 (2020)
Translated by M.A. Monastyrskiy

the polylactide basis by the methods of supercritical fluid (SCF) foaming in supercritical CO_2 (SC CO_2) environment and surface-selective laser sintering (SSLS) were selected [6, 21, 22]. In both cases, classical models of matrices possessing an interconnected pore system were used. In the first case, the pores are formed randomly as a result of fluid release from the swollen polymer, while in the second case, the polymer scaffold formation occurs in accordance with a given computer model. For the formation of both types of structures (foaming in SC CO_2 and sintering), polylactide was employed, which is one of the most often used materials for the formation of tissue-engineering constructs [23–27].

The purpose of this work is to estimate the intensity distribution of low-intensity light in the visible and near-IR spectral regions in three-dimensional porous polylactide scaffolds fabricated by foaming in SC CO_2 and surface-selective laser sintering.

2. Materials and methods

In the experiment, polylactide scaffolds fabricated by two methods [6] were used: SCF foaming in the SC CO_2 environment [21] and surface-selective laser sintering [22].

In the first case, porous polymer scaffolds were obtained by foaming copolymers of D, L -lactide and ε-caprolactone (4 mol%) in the SC CO_2 environment in accordance with the technique [21]. The foamed samples were formed in the SC CO_2 environment using an installation developed at the IPT RAS [6, 21, 28]. The initial copolymer in the form of a powder with particles of 100–200 μm in size and 400 mg in weight was placed in a fluoropolymer form, which was installed in the reactor of the setup. For optical experiments, a scaffold with a diameter of 8 mm and a thickness of 1.2 mm was cut from the sample.

As a material for producing scaffolds by the SSLS method [6, 22], the PDL 02A (Corbion) polylactide was used in the form of a powder with a particle size up to 100 μm. To increase the hydrophilicity, the material was kept in a 1% solution of hyaluronic acid and dried using a FreeZone Plus 2.5 (LABCONCO) lyophilisation unit. Water was used as a sensitiser. For optical experiments, a sample with a diameter of 8 mm and a thickness of 1.2 mm was formed.

Optical characteristics of dry and wet samples were studied. Wet samples were obtained by incubation in distilled water for 24 hours. Changes in the optical characteristics of wet samples, caused by the evaporation of water during a few minutes of the experiment, were not taken into account.

A scheme of the original setup for determining the optical characteristics of scaffolds [6, 29] is shown in Fig. 1.

The setup is based on two integrating spheres (*1*) and (*2*) with a diameter of 75 mm, coated from the inside with a standard diffusely scattering material. The spheres were installed strictly coaxially with collimators (*5*) and (*6*). Using a special holder (*8*), a scaffold sample (*7*) was located between the spheres and illuminated by a uniform beam of light with a diameter of 4.8 mm from a source (*3*) connected to collimator *5* by an optical fibre. An HL-2000 (Ocean Optics, USA) halogen source was used as a light source. The back-scattered light reflected from the front surface of the sample is collected by integrating sphere *1*. The light diffusely passing through the sample was collected by integrating sphere *2*. The light that passed through the sample without deflection fell on collimator *6*. Using the USB4000 spectrometer (Ocean Optics, USA) with a wavelength range of 200–1100 nm, the light spectra were measured within two spheres and at the output of collimator *6*.

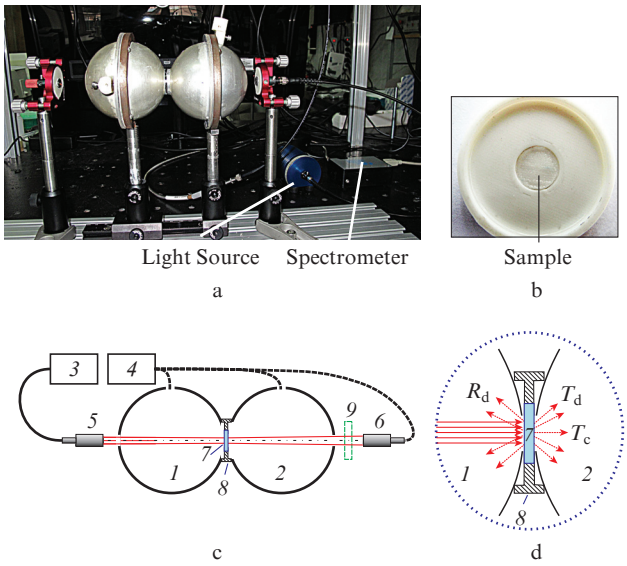

Figure 1. Setup for determining the optical characteristics of scaffold samples: (a) external view; (b) scaffold sample in the holder; (c) schematic of the setup [(*1*, *2*) integrating spheres; (*3*) broadband light source; (*4*) spectrometer; (*5*, *6*) collimators; (*7*) sample; (*8*) sample holder; (*9*) neutral filter]; (d) sample location on an enlarged scale (arrows conventionally show diffuse, reflected, and diffusely transmitted light, the intensities of which are used to calculate the spectra of diffuse scattering R_d, diffuse transmittance T_d and collimated transmittance T_c).

The data obtained allowed us to calculate the spectra of the coefficients of diffuse scattering R_d, diffuse transmission T_d, and collimated transmission T_c:

$$R_d = I_1/I_{10},\ T_d = I_2/I_{10},\ T_c = I_3/I_{30}, \quad (1)$$

where I_1 is the light intensity in sphere *1* with the sample; I_{10} is the light intensity in sphere *1* when its output aperture is closed by a standard plug with a diffusely scattering coating; I_2 is the intensity in sphere *2* (with a sample) when its output is closed by a standard plug; I_3 is the intensity at the output of collimator *6*; and I_{30} is the intensity at the output of collimator *6* in the absence of the sample. When measuring I_{30}, an NGG10 neutral filter (*9*) was installed in front of collimator *6* to attenuate the light. Then, the measurement results were recalculated with regard to the transmission spectrum of the neutral filter.

Because of the smallness of the absorption coefficient μ_a of polylactide, the scattering coefficient μ_s was determined from the value of the collimated transmittance T_c: $\mu_s = \ln(T_c)/d$, where d is the scaffold sample thickness. Then, using the modernised Monte Carlo method [18, 20], a direct problem was solved with the Matlab software package. For this purpose, stochastic trajectories of photon packets incident on the sample perpendicular to its surface and forming a homogeneous beam with a diameter of 5.0 mm were calculated. It was assumed that the probability density of the scattering angle is described by the Henyey–Greenstein function [18, 20], which only depends on the average cosine of the scattering angle (anisotropy factor *g*).

The programme enabled us to find the absorbed light energy distribution in the sample volume and determine R_d and T_d in accordance with the set values of the μ_s and μ_a coefficients, the refractive indices of polylactide, water and air, and the porosity of the scaffolds. At small μ_a values, the absorbed energy in each volume element corresponds to the desired fluence rate. By varying g, we can find the R'_d and T'_d values that provide the best agreement with the experiment. To this end, it is necessary to determine a minimum of the expression

$$\Delta = \frac{(R'_d - R_d)^2}{R_d^2} + \frac{(T'_d - T_d)^2}{T_d^2}. \quad (2)$$

The density distributions of the absorbed light energy in the sample volume, calculated using the Henyey–Greenstein function and the geometric function of scattering on spherical cavities, were compared. In the case of a porous structure (with small spherical bubbles), the probability density of the scattering angle only depends on the refractive indices of the material and the bubbles, assuming that the scattering of photons occurs according to Fresnel's law.

The polylactide refractive index was calculated using a well-known expression [27] valid in the wavelength range of 300–1300 nm:

$$n = (1.44500 \pm 0.00075) + (4892 \pm 143)\ (\text{nm}^2\,\lambda^{-2}). \quad (3)$$

In the range $\lambda = 500$–900 nm, in accordance with (3), the polylactide refractive index is $n = 1.4559 \pm 0.003$. In the entire studied range, the changes in n did not exceed ±0.26%, which is significantly less than the error of experimental measurements.

The absorption coefficient of the polylactide film was determined. To this end, polylactide crumbs were dissolved in dichloromethane; the solution was applied to the cover glass and dried in air until a film with a thickness of 125 μm was formed. The absorption spectrum was measured with a Varian Cary 50 Scan spectrophotometer; the average value of the absorption coefficient in the range from 500 to 900 nm constituted 0.28 ± 0.11 cm^{-1}.

A PHENOM ProX (Phenom World, Netherlands) scanning electron microscope was used to visualise the porous structure of the sample material.

3. Results and discussion

Figure 2 shows the external view of samples of two matrices in holders and SEM images of their slices. It can be seen that the structures of the samples obtained by different methods vary significantly. In scaffold 1 (foaming in SC CO_2), relatively large pores (up to 300 μm) are formed (Fig. 2a); outside these pores, the polylactide structure is quite homogeneous. In sample 2 (sintering), rounded polylactide grains are distinguished (Fig. 2b). The pores between these grains reach ~100 μm. At the same time, the polylactide structure in the grains themselves, as can be seen from several slices, is finely porous. The porosity of the matrix material, determined by SEM images of the slices, was 70% ± 4% for sample 1 and 62% ± 3% for sample 2.

The μ_s spectra calculated from the spectra of the coefficients T_c of collimated transmission are shown in Fig. 3. As can be seen from this Figure, for different samples in dry and wet states, the shapes of the spectra obtained qualitatively coincide, though their levels differ significantly. In the course

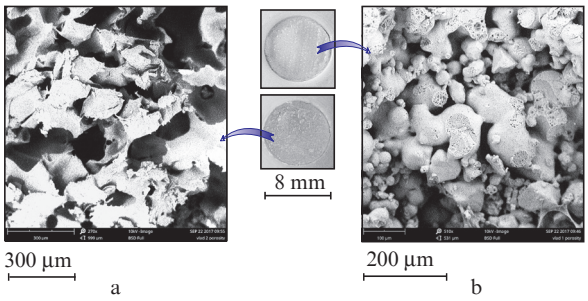

Figure 2. Scaffold samples obtained by (a) foaming and (b) sintering (optical images of samples in holders and areas of SEM images are shown).

of transition from dry to wet samples, the μ_s value in the entire spectral range decreases by approximately the same value for each of the samples. On average, this decrease for sample 1 constitutes 17%, and for sample 2, 10%. The highest μ_s values were recorded for dry sample 2 obtained by surface-selective laser sintering, the lowest, for wet sample 1 formed by foaming in SC CO_2.

The spectra of the coefficients of diffuse scattering R_d and

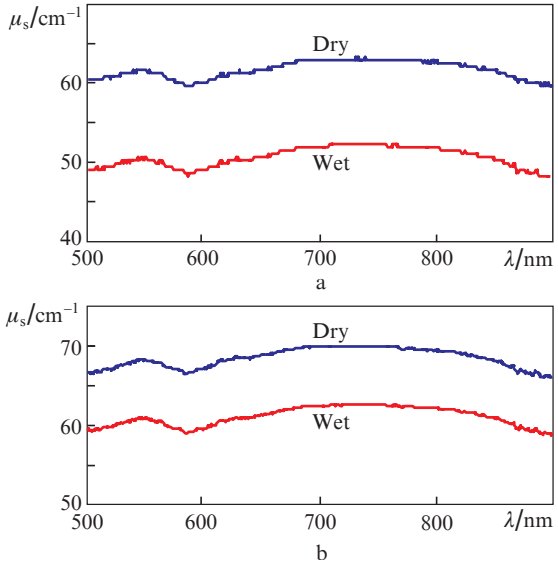

Figure 3. Spectra of μ_s for dry and wet matrices obtained by (a) foaming in SC CO_2 and (b) laser sintering.

diffuse transmission T_d, obtained using the integrating sphere, are shown in Fig. 4. It is seen that the obtained values of R_d and T_d for dry and wet samples are weakly dependent on the wavelength. At the same time, their values differ significantly. During the transition from dry to wet samples, the R_d value in the entire spectral range decreases, while the T_d value increases. On average, the decrease in R_d for sample 1 is significant and amounts to 67%, while for sample 2 it only constitutes 12%. The increase in T_d was on average 73% for sample 1 and 104% for sample 2. The highest R_d values were recorded for dry sample 2, while the lowest, for wet sample 1. At the same time, the highest T_d values were recorded for wet sample 1, while the lowest, for dry sample 2.

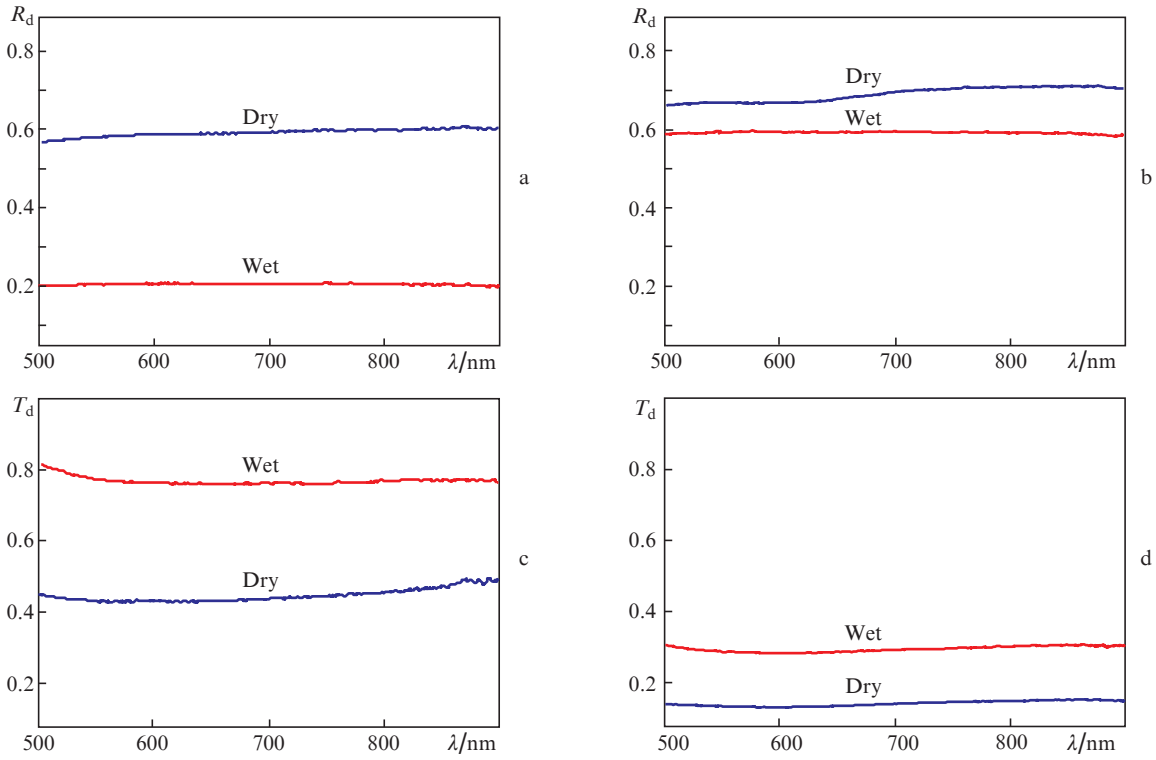

Figure 4. Spectra of the coefficient of (a, b) diffuse scattering R_d and (c, d) transmission T_d for dry and wet scaffolds obtained by (a, c) foaming in SC CO_2 and (b, d) laser sintering.

Table 1 shows the experimentally obtained values of the coefficients of diffuse scattering R_d, diffuse transmission T_d, and collimated transmission T_c, as well as the calculated values of the anisotropy factor g for samples of dry and wet scaffolds fabricated by various methods. The lowest values of the anisotropy factor ($g = 0.3 \pm 0.05$) were obtained for dry sample 2, and the highest values ($g = 0.85 \pm 0.1$), for wet sample 1.

Table 1. Experimentally obtained values of the coefficients of scattering μ_s, diffuse scattering R_d, diffuse transmission T_d, collimated transmission T_c and calculated values of the anisotropy factor g for dry and wet samples fabricated by various methods ($\lambda = 633$ nm).

Parameter	Sample 1 (foaming in SC CO_2)		Sample 2 (laser sintering)	
	Dry	Wet	Dry	Wet
μ_s/cm^{-1}	61 ± 1	50 ± 2	69 ± 1	61 ± 2
R_d	0.59 ± 0.01	0.20 ± 0.01	0.69 ± 0.02	0.60 ± 0.01
T_d	0.45 ± 0.02	0.76 ± 0.01	0.14 ± 0.01	0.28 ± 0.01
$T_c/10^{-5}$	64 ± 2	240 ± 10	27 ± 1	67± 2
g	0.6 ± 0.1	0.85 ± 0.10	0.30 ± 0.05	0.45 ± 0.11

Using the obtained optical parameters of the sample materials, the density distributions of the absorbed light energy inside the samples, linearly related to the fluence rate, were calculated. Below, the term intensity means the fluence rate (Fig. 5).

The obtained dependences of the light intensity in the samples on the depth (the distance from the surface onto which light falls with intensity $I = 1$) are qualitatively similar. It can be seen that with increasing depth, the intensity

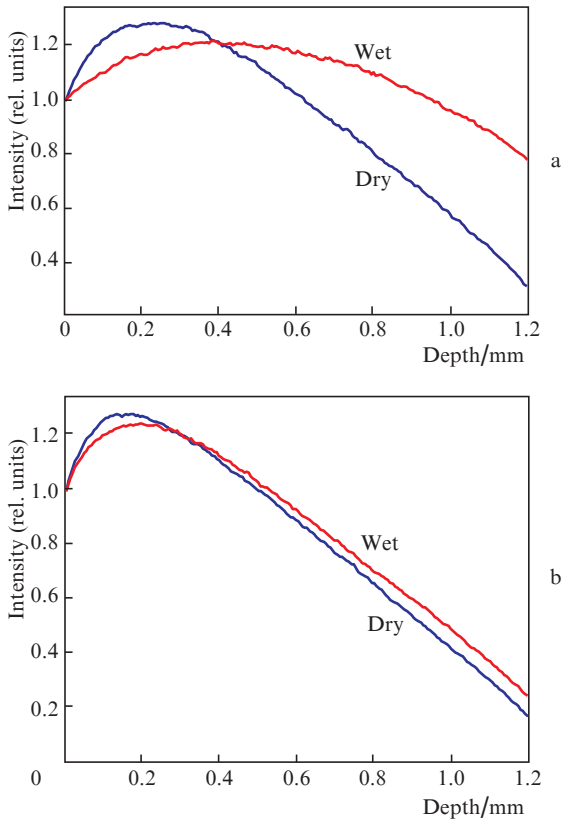

Figure 5. Intensity distributions of laser light with $\lambda = 633$ nm inside dry and wet samples obtained by (a) foaming in CO_2 and (b) laser sintering. The distributions are calculated using the Monte Carlo method.

increases, and then, having reached its maximum value, monotonously decreases. Wetting the scaffolds leads to a decrease in the maximum intensity value, an increase in the depth of reaching this maximum, and a smaller slope of the curve in the region of monotonous intensity decrease. For scaffold 1, these changes are as follows: The maximum intensity value decreases from 1.28 to 1.21 (by 5%), the depth of reaching the maximum light intensity increases from 0.23 to 0.40 mm (by 73%), the curve slope in the region of monotonous intensity decrease reduces from 40° up to 29°(by 28%). For scaffold 2, the changes are: The maximum intensity decreases from 1.28 to 1.24 (by 3%), the depth of reaching the maximum light intensity increases from 0.15 to 0.20 mm (by 33%), the curve slope in the region of monotonous intensity decrease reduces from 40° to 39° (by 2.5%).

The obtained regularities of the distribution of incident light intensity in polylactide scaffolds are qualitatively consistent with the results for other strongly scattering media derived as a result of calculation using the Monte Carlo method [17–20] or by direct measurements [30]. In the case of predominant scattering, as the distance from the surface increases, the light intensity initially increases, and then, upon reaching a maximum, monotonously decreases. In the case of wet samples, when the pores are filled with water, μ_s value decreases, which leads to an increase in the anisotropy factor g and 'clearing' of the sample. At first glance, it seems paradoxical that, at approximately the same porosity (70% ± 4% for sample 1 and 62% ± 3% for sample 2), wetting of sample 2 resulted in a significantly smaller change in μ_s (see Fig. 3, Table. 1) and a smaller difference in the profile of light intensity distribution over the sample depth (Fig. 5). However, if we refer to SEM images of the samples (see Fig. 2), we can see a significant difference in their structures. The polylactide structure in sample 1 is homogeneous outside the large (up to 300 μm) pores, while in sample 2 the structure in grains (outside the large ones) is finely porous. The porosity of this fine-grained structure of the second sample estimated by SEM images constituted 30% ± 3%. If only large pores are filled, while small pores in the grains remain unfilled, this may explain the not very significant change in optical scattering in the second sample when it is wetted with water.

The light fields calculated using the Henyey–Greenstein phase scattering function were compared with a numerical model of light scattering by a spherical cavity at the same g = 0.56 (Fig. 6); this value corresponds to the polylactide refractive index n = 1.4559. The model phase scattering function is a probability density of the angle of the light beam deflection by a spherical cavity, calculated from the geometric representations of the path of light rays and Fresnel formulas for the refraction and reflection coefficients. This model allows for multiple reflections inside the cavity. The scattering indicatrices for the Henyey–Greenstein function and the numerical model of light scattering by a spherical cavity at an average cosine of the deflection angle of 0.56 are shown in the inset to Fig. 6a. Note that the model phase scattering function for a spherical cavity only depends on the relative refractive index and does not depend on the cavity diameter.

As can be seen from Fig. 6, the light field intensity distributions calculated by the two methods are virtually identical. The maximum discrepancy that is observed in the region of the curve maxima (Figs 6a and 6c) does not exceed 4%. In principle, this result is expectable for multiple scattering of light in a weakly absorbing medium. An important circumstance in this case is the equality of the average cosines of the

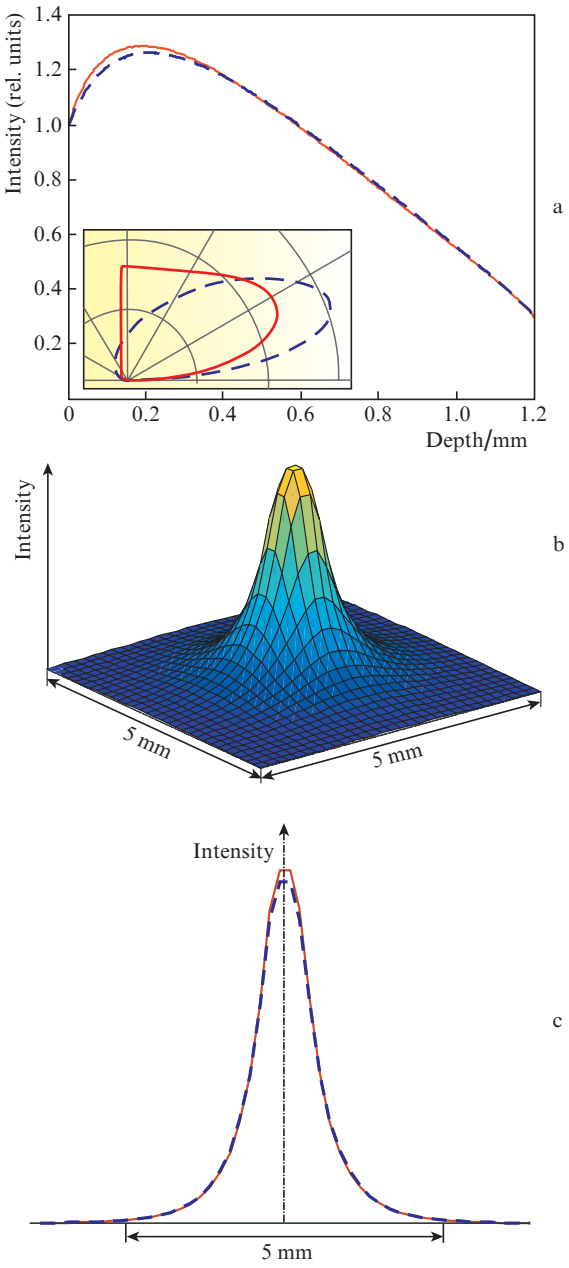

Figure 6. Laser light intensity distributions in dry scaffold 1, obtained using (dashed curves) the Henyey–Greenstein function and (solid curves) a numerical model of light scattering by a spherical cavity with g = 0.56: (a) change in intensities with distance from the surface (the inset shows the scattering indicatrices for two methods); (b) intensity distribution at a depth of 0.54 mm, constructed on the basis of a numerical model of light scattering by a spherical cavity; (c) profiles of intensity distributions at a depth of 0.54 mm, calculated by two methods.

light beam deflection angles. Apparently, the energy distribution of a light beam in a weakly absorbing but strongly scattering medium is mainly determined by the average angle of light deflection during scattering, while other details of the phase scattering function become less significant or negligible. The Henyey–Greenstein phenomenological phase scattering function is often used to estimate the light propagation in scattering media, especially in biological tissues. For comparison, we also used a numerical model of light scattering by a spherical cavity, which is physically justified to a certain extent. There are also other phase scattering functions for

optically inhomogeneous media, among which the probability density of the angle of light deflection by a randomly oriented interface between two media with different refractive indices may be of interest [31, 32].

4. Conclusions

Fluence rate distributions in three-dimensional porous polylactide matrices fabricated by the methods of SCF foaming and surface-selective laser sintering have been determined by irradiating the samples with a collimated light beam. This information is relevant for tissue engineering when choosing the optimal parameters for laser stimulation of cells located in polymer scaffolds. It is shown that the anisotropy factor g and scattering coefficient μs are the determining parameters for the light field formation in the case of strongly scattering media.

Acknowledgements. The authors are grateful to N.V. Minaev for his assistance in designing the setup, and N.N. Vorob'eva and S.N. Churbanov for preparing the samples.

This work was supported by the Ministry of Science and Higher Education in the framework of the State Assignment of the Federal Scientific Research Centre 'Crystallography and Photonics' of the Russian Academy of Sciences in part of the development of laser technologies, as well as the Russian Foundation for Basic Research (Grant No. 17-02-00832, 17-02-01248, and 18-29-06056) in part of photonics and supercritical fluids.

References

1. Nerem R.M., Sambanis A. *Tissue Eng*., **1** (1), 3 (1995).
2. Lanza R., Langer R., Vacanti J.P. *Principles of Tissue Engineering* (London: Elsevier/Academic Press, 2014).
3. Dvir T., Timko B.P., Kohane D.S., Langer R. *Nat. Nanotechnol.,* **6**, 13 (2011).
4. Ivanov A.N., Norkin I.A., Puchin'ian D.M. *Tsitologiia*, **56** (8), 543 (2014).
5. Radisic M., Deen W., Langer R., Vunjak-Novakovic G. *Am. J. Physiol. Heart Circ. Physiol*., **288** (3), H1278 (2005).
6. Yusupov V.I., Sviridov A.P., Zhigarkov V.S., Shubnyy A.G., Vorobieva N.N., Churbanov S.N., Minaev N.V., Timashev P.S., Rochev Y.A., Bagratashvili V.N. *Proc. SPIE,* **10716**, 107161U (2018).
7. Baxter G.D. *Therapeutic Lasers: Theory and Practice* (New York: Churchill Livingstone, 1994).
8. Tuner J., Hode L. *Low Level Laser Therapy – Clinical Practice and Scientific Background* (Spjutvagen: Prima Books, 1999).
9. Chung H., Dai T., Sharma S.K., Huang Y.Y., Carroll J.D., Hamblin M.R. *Ann. Biomed. Eng*., **40** (2), 516 (2012).
10. Karu T.I. *Ten Lectures on Basic Science of Laser Phototherapy* (Grangesberg: Prima Books, 2007).
11. Andreeva N.V., Zotov K.V., Egorov E.E., Kandarakov O.F., Yusupov V.I., Bagratashvili V.N., Belyavskii A.V. *Molek. Biol*., **52** (6), 1014 (2018).
12. Iwase T., Hori N., Morioka T., Carpenter D.O. *Laser Surg. Med*., **19** (4), 465 (1996).
13. Chailakhyan R.K., Yusupov V.I., Gorskaya Yu.F., Kurolesova A.I., Gerasimov Yu.V., Sviridov A.P., Tambiev A.Kh., Vorobyeva N.N., Grosheva A.G., Shishkova V.V., Moskvina I.L., Bagratashvili V.N. *J. Innov. Opt Health Sci*., **10** (1), 1650036 (2016).
14. Osipova E.A., Krylov V.V., Yusupov V.I. *Zh. Sibir. Federal. Univer., Biol*., **3**, 301 (2011).
15. Zaichkina S.I., Dyukina A.R., Rozanova O.M., Simonova N.B., Romanchenko S.P., Sorokina S.S., Zakrzhevskaya D.T., Yusupov V.I., Bagratashvili V.N. *Bull. Eksp. Biol. Med.*, **161** (1), 32 (2016).
16. Zhu W., George J.K., Sorger V.J., Grace Zhang L. *Biofabrication*, **9** (2), 025002 (2017).
17. Niemz M.H. *Laser-Tissue Interactions: Fundamentals and Applications* (Springer, Science & Business Media, 2013).
18. Welch A.J., van Gemert M.J., Star W.M., in O*ptical-Thermal Response of Laser-Irradiated Tissue* (Dordrecht: Springer, 2011) pp 27–64.
19. Tuchin V.V. *Usp. Fiz. Nauk*, **167**, 917 (1997).
20. Tuchin V.V., Maksimova I.L., Zimnyakov D.A., Kon I.L., Mavlyutov A.H., Mishin A.A. *J. Biomed. Opt*., **2** (4), 401 (1997).
21. Timashev P.S., Vorobieva N.N., Minaev N.V., Piskun Y.A., Vasilenko I.V., Lakeev S.G., Bagratashvili V.N. *Russ. J. Phys. Chem. B*, **10** (8), 1195 (2016).
22. Antonov E.N., Krotova L.I., Minaev N.V., Minaeva S.A., Mironov A.V., Popov V.K., Bagratashvili V.N. *Quantum Electron*., **45** (11), 1023 (2015) [*Kvantovaya Elektron*., **45** (11), 1023 (2015)].
23. Maquet V., Martin D., Malgrange B., Franzen R., Schoenen J., Moonen G., Jérôme R. *J. Biomed. Mater. Res., Part A*, **52** (4), 639 (2000).
24. Sachlos E., Czernuszka J.T. *Eur. Cells Mater*., **5** (29), 39 (2003).
25. Van Sliedregt A., Radder A.M., De Groot K., Van Blitterswijk C.A. *J. Mater Sci. Mater. Med*., **3** (5), 365 (1992).
26. Ahmed J., Varshney S.K. *Int. J. Food Prop*., **14** (1), 37 (2011).
27. Hutchinson M.H., Dorgan J.R., Knauss D.M., Hait S.B. *J. Polym. Environ*., **14** (2), 119 (2006).
28. Minaev N.V., Antonov E.N., Minaeva S.A., Churbanov S.N. *Prib. Tekh. Eksp*., **1**, 150 (2019).
29. Yusupov V.I., Minaev N.V., Sviridov A.P. *Prib. Tekh. Eksp*., **6**, 130 (2019).
30. Karabutov A.A., Pelivanov I.M., Podymova N.V., Skipetrov S.E. *Pis'ma Zh. Eksp. Teor. Fiz*., **70** (3), 187 (1999).
31. Sviridov A.P. *Quantum Electron*., **37**, 1 (2007) [*Kvantovaya Elektron*., **37**, 1 (2007)].
32. Sviridov A.P. *Proc SPIE*., **6164**, 61640D (2005).